

X-RAY COMPUTED TOMOGRAPHY INSPECTION OF THE STARDUST HEAT SHIELD (IPPW-7)

Karen M. McNamara⁽¹⁾, Daniel J. Schneberk⁽²⁾, Daniel M. Empey^{(3)*}, Ajay Koshti⁽¹⁾, D. Elizabeth Pugel⁽⁴⁾, Ioana Cozmuta⁽⁵⁾, Mairead Stackpoole⁽⁵⁾, Norman P. Ruffino⁽⁶⁾, Eddie C. Pompa⁽⁶⁾, Ovidio Oliveras⁽⁶⁾ and Dean A. Kontinos⁽⁷⁾

⁽¹⁾NASA Johnson Space Center, ⁽²⁾Lawrence Livermore National Labs, ⁽³⁾Sierra Lobo, Inc., ⁽⁴⁾NASA Goddard Space Flight Center, ⁽⁵⁾Eloret Corporation, ⁽⁶⁾Jacobs Technology, ⁽⁷⁾NASA Ames Research Center

ABSTRACT

The “Stardust” heat shield, composed of a PICA (Phenolic Impregnated Carbon Ablator) Thermal Protection System (TPS), bonded to a composite aeroshell, contains important features which chronicle its time in space as well as re-entry. To guide the further study of the Stardust heat shield NASA reviewed a number of techniques for inspection of the article. The goals of the inspection were: 1) to establish the material characteristics of the shield and shield components, 2) record the dimensions of shield components and assembly as compared with the pre-flight condition, and 3) through the evaluation of the shield material provide input to future missions which employ similar materials.

Industrial X-Ray Computed Tomography (CT) is a 3D inspection technology which can provide information on material integrity, material properties (density) and dimensional measurements of the heat shield components. Computed tomographic volumetric inspections can generate a dimensionally correct, quantitatively accurate volume of the shield assembly. Because of the capabilities offered by X-ray CT, NASA chose to use this method to evaluate the Stardust heat shield.

Personnel at NASA Johnson Space Center (JSC) and Lawrence Livermore National Labs (LLNL) recently performed a full scan of the Stardust heat shield using a newly installed X-ray CT system at JSC. This paper briefly discusses the technology used and then presents the results of the scans obtained along with comparisons of the scan data with data obtained from samples cut from the heat shield as well as comparisons with the as-built dimensions. Density variation, “char” layer thickness, recession and bond line (the adhesive layer between the PICA and the aeroshell) integrity are all evaluated. Finally suggestions are made as to future uses of this technology as a tool for non-destructively inspecting and verifying both pre and post flight heat shields.

1. INTRODUCTION

The recently returned “Stardust” heat shield contains important features which chronicle its time in space as well as re-entry. To guide the further study of the Stardust shield NASA reviewed a number of non-destructive techniques for inspection of the shield. The goals of the inspection are: 1) to establish the material characteristics of the shield and shield components, 2) record the dimensions of shield components and assembly as compared with the pre-flight condition, and 3) through the evaluation of the shield material provide input to future missions which employ similar materials.

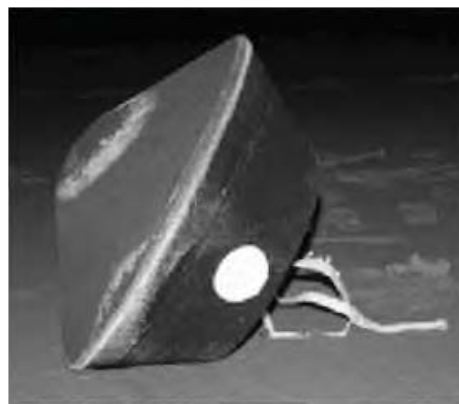


Fig. 1 - Stardust Capsule.

Industrial X-Ray Computed Tomography is a 3D inspection technology which can provide information on material integrity and dimensional measurements of shield components and component materials. Computed tomographic volumetric inspections can generate a dimensionally correct, quantitatively accurate volume of the shield assembly. CT reconstructed data is comprised of volume elements or “voxels” at each 3D position in the volume covering the object under inspection. For x-ray based CT the voxel is in units of x-ray attenuation, relative attenuation for polychromatic sources and total attenuation for mono-chromatic sources; the product of

chemical formula and density. Consequently, voxel intensities measure changes in material composition and can be used to measure dimensions of features, anomalies and/or component structures.

NASA JSC has recently completed the construction of an x-ray cell facility that includes two x-ray sources and two detectors. The two x-ray sources are a COMET 450 KVp tube with focal spots of 0.4 and 1.0 mm, and a 150 KVp Hamamatsu Micro-Focal source with three choices of x-ray spot (0.05, 0.01 and 0.005 mm nominal). The COMET tube head is on a manually translatable rail which supports source-to-detector distances from 4 to 12 feet. The Hamamatsu micro-focal source resides on the 4 ft by 6 ft optical table with the THALES Amorphous Silicon detector, enabling precise positioning for high-cone angle techniques. Up to three different NEWPORT motion stages are also on the optical table to support different Computed Tomography and Laminographic scanning methodologies. Taken as a whole, the two x-ray sources, the manual and computerized motion; the JSC X-ray capability can scan a large variety of objects, at a wide range of spatial resolutions, and employing a range of scanning techniques.

2. SCANNING METHODOLOGY

The diameter of the Stardust shield is 81 cm (32 in.) with the overall shape of a blunted 60° half angle sphere cone.. Further, the Stardust shield can be described as constituted of 3 layers; 1) an outer PICA

layer, 2) an Aluminum honeycomb layer and 3) a support substructure of aluminum posts and interior cross-members. Inspection questions span the different components of the shield; what is the material state of the PICA, what is the material thickness, and is this thickness greater or less in different parts of the shield? Is there a change in the material composition of the PICA close to the exterior surface? What is the magnitude of this change? Are there any unexpected anomalies in the Aluminum honeycomb? And, what is the state of the bond-line between the PICA and the Aluminum honeycomb.

The 450 kVp scanning system at JSC includes motion can accommodate 4 different scanning modes. Figure 2 contains the different alternatives. Given the large size of the Stardust shield as compared to the 40 by 30 cm (approximately 16 by 12 in.) size of the Flashscan 33 detector, we elected to implement a ‘‘tiled-scan’’ strategy. The impact of this choice is rather long scan times; the total scan time equals the time for a single scan multiplied by the number of tiles. Secondly, there is the added complexity of positioning the detector with sufficient precision to construct a ‘‘joined’’ scan that does not include artifacts from the ‘‘joining’’ operation. The source-detector geometry for the JSC 450 kVp room is cone-beam, requiring the detector be moved to cover the entire projected size of the Stardust shield at the detector plane. To reduce the number of tiles we elected to scan with ‘‘half-scan’’ or ‘‘offset-scan’’ techniques where we reconstruct the entire object from a field of view that covers just over half of the

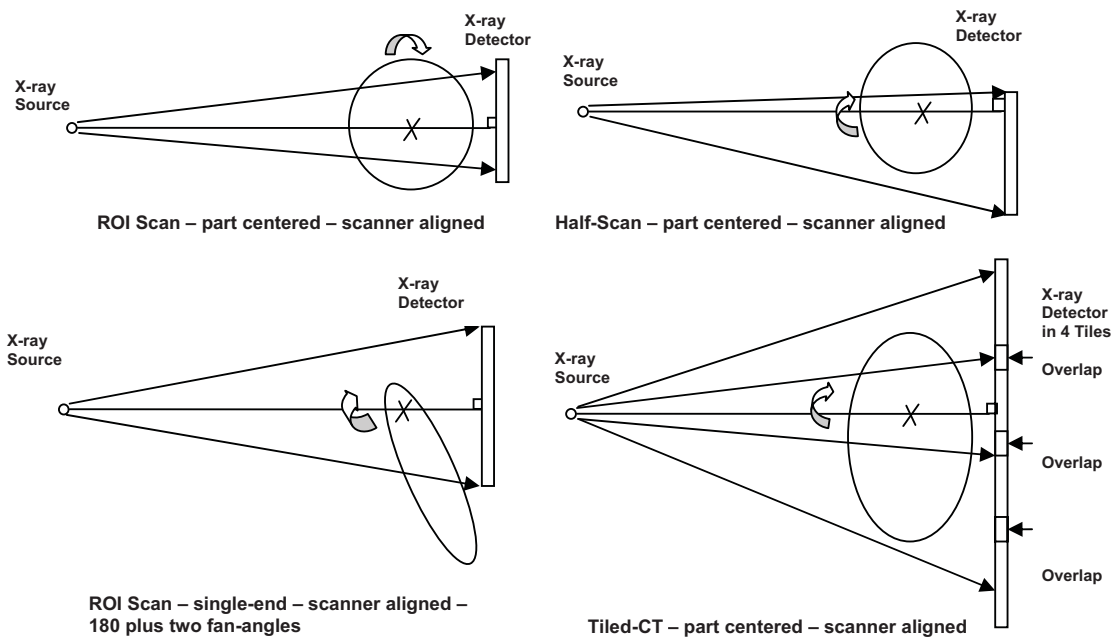


Fig. 2 - Alternative scanning modes at JSC.

object. These two techniques result in a scan comprised of three separate “scan-tiles”, which when joined together and reconstructed produce a 3D CT volumetric inspection data set for the Stardust shield.

Selected scan parameters for each of the tiled scans represent a choice among competing constraints. The virtual detector is built up from the different scans, resulting in large data sets. Consequently, the number of rotational views acquired should be sufficient for the constructed detector, not any one tile. It is important to note also that increasing the number of views increases scan time by the number of tiles. Secondly, alignment tolerances get more critical with cone-angle which increases the amount of precision for positioning the detector. Third, we are interested in substantial spatial resolution, which means the source unsharpness (the blur due to the finite size of the source spot) needs to be kept under control. These constraints given, we elected to scan the shield with 900 views over 360 degrees. We are looking for spatial resolution in the 0.3-0.5 mm range, consequently we chose to position the source-object-detector in a low-cone, low-magnification configuration. The source to detector distance was set at 3048 mm, with a source to object distance of 2591 mm, an x-ray magnification of 1.176. The amorphous silicon detector was operated in the 1.5 binning mode, resulting in a detector size of 0.1905 mm at the detector, and with this magnification, the voxel size for the reconstructed volume could be as low as 0.162 mm. For the virtual detector, comprised

of the 3 tiles, the field of view was roughly 570 mm, resulting in a cone angle of this configuration resulted in a cone-angle of 9.4 degrees. Using the small spot from the COMET tube head of 0.4 mm, the estimated size of the source unsharpness at the object for this magnification is 0.0704 mm, easily less than the 0.162 mm minimum voxel size for the reconstructed volume. Each of the three 900 view scans was acquired separately with the detector moved in-between scans. Referring to Fig. 2, the center section scan comprised a ROI scan, and was acquired first to enable a center-reconstruction to be processing while the other scan-tiles were being acquired. Fig. 3 contains individual radiographs with the joined radiograph displayed in Figure 4. Fig. 5 contains a vertical slice from the reconstructed volume for the Stardust heat shield inspection.

All 900 radiographs in the three tiles were joined into a radiograph as displayed in Fig. 4. Those 900 radiographs acquired over 360 degrees were then processed and reconstructed with a modified Feldkamp reconstruction algorithm for the “offset-scan” geometry illustrated by the radiograph in Fig. 5. In the course of processing the data we resampled the projection data to support a reconstruction into 0.324 mm cubic voxels (the 0.162 mm pixel radiographs were resampled 2x2). The result is a 2640 by 2640 by 1000 volume of voxel elements.

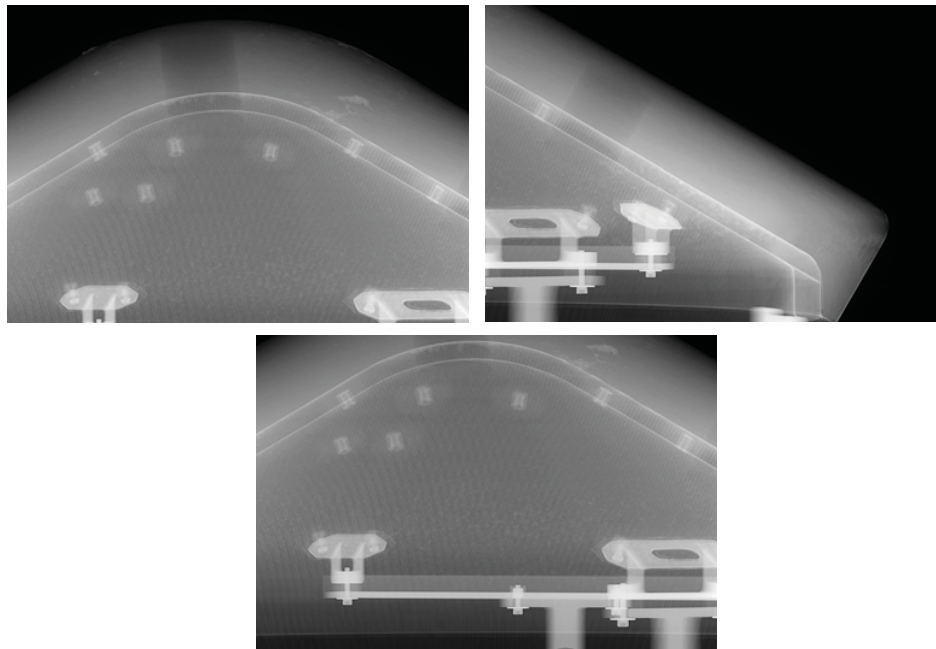


Fig. 3 - First images from the three acquired scans.

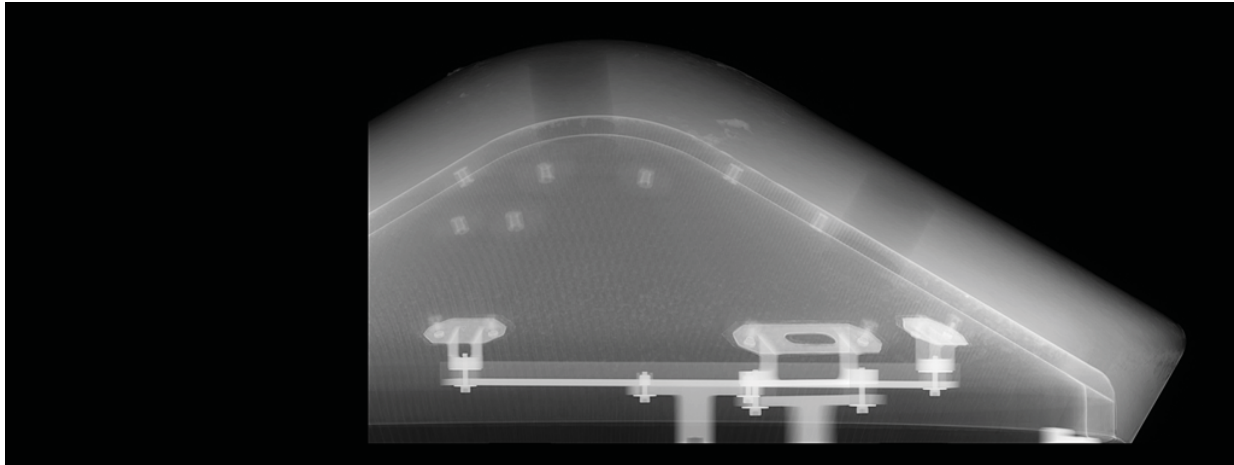


Fig. 4 - Joined digital radiograph from three tiled scans.

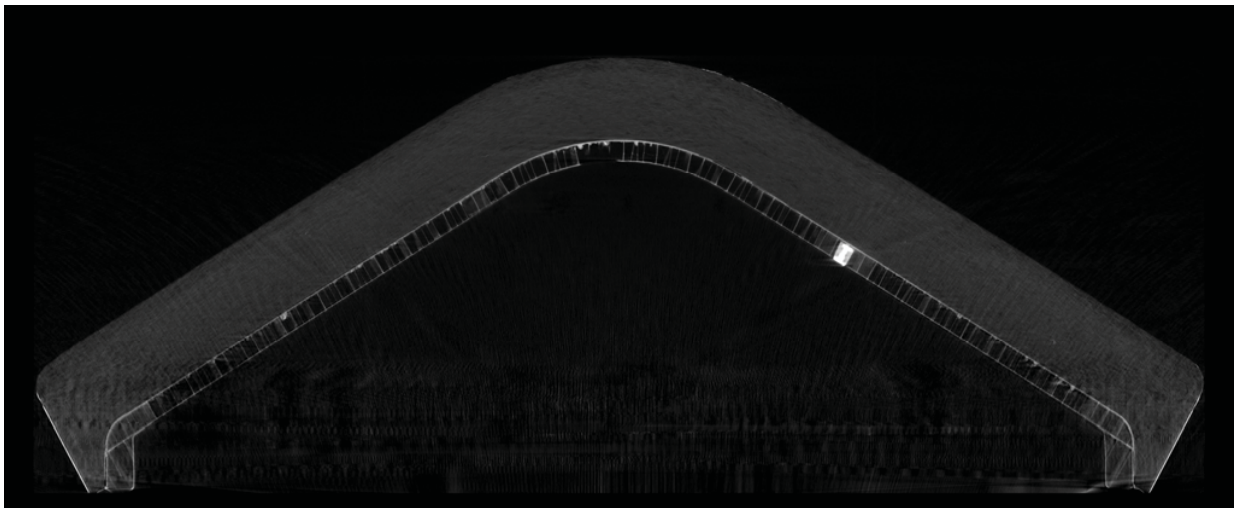


Fig. 5 - Vertical slice from tiled offset-scan.

The vertical slice shown in Fig. 5 shows two of the main components of the stardust shield, the PICA and the aluminum honeycomb underneath. Also, notice some structured noise or artifacts in the lower part of the vertical slice in Fig. 5 which are a combination of “streak” artifacts (from the long chords in the Aluminum and the inadequate number of views for a radiographic area of this size). Fig. 6 contains a close-up view of the center-top of the vertical slice from the reconstructed volume showing the type of detail imaged by the CT scanning in the JSC system. Using the different Aluminum pieces, and the drilled holes in the Stardust Shield as reference standards, the volume appears to include accurate dimensions of the internals of the Stardust shield.

3. REVIEW AND ANALYSIS OF 3D VOLUMETRIC DATA

The 3D CT data can be viewed and unpacked in a number of different ways from a number of different orientations. Fig. 7 contains a cross-sectional or (transverse) slice through the Stardust reconstructed volume. In both Fig. 6 and Fig. 7, notice the texture in the slices through the PICA, we consider this texture in the images to be an accurate measure of the variation of the fibers in the make-up of the PICA. Also, there appears to be higher attenuating material sparsely interspersed within PICA material. Preliminary analysis of these higher-attenuating chunks indicate a close resemblance to the same features found in scans of recently fabricated PICA [1]. Second, notice the

small change in attenuation in the cross-sectional slices towards the outside boundary of the PICA, we consider this change in attenuation to be the char layer, a feature we will examine subsequently. Third, for the slices showing the state of the Aluminum honeycomb, notice a variation in the attenuation in the interstitial layer between the honeycomb and the PICA. It appears there are gaps in the fill between the PICA and the Aluminum honeycomb. Fourth, there appears to be higher attenuating material on the outside of the PICA. From a visual inspection of the outside of the shield, this is “dirt” accumulated on the shield from the landing. As expected the “dirt” is higher in x-ray attenuation than the PICA. Lastly, notice the hole cut

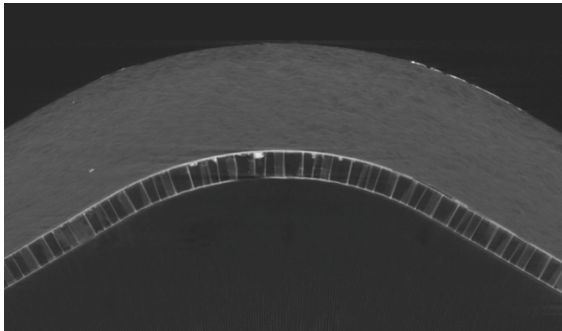


Fig. 6 - Extracted region from verticle CT slice.

in the PICA from some destructive analysis work. This feature provided a useful reference for verifying the dimensional accuracy of our reconstructed volume.

Four questions have been identified as important for the analysis of the Stardust Shield; 1) what is the thickness of the PICA layer, and how does it compare to the as-built state of the shield, 2) are there anomalies

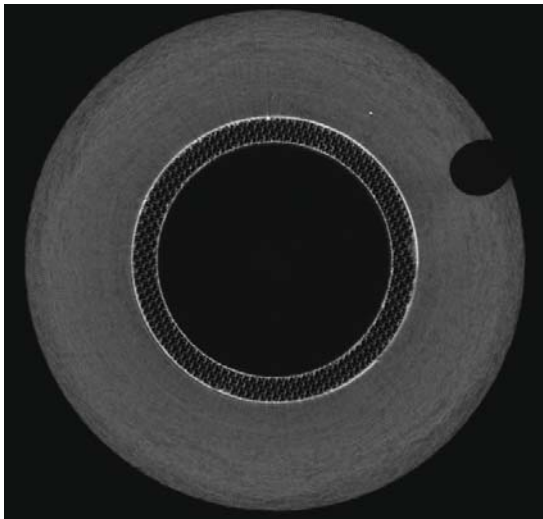


Fig. 7 - Transverse CT slice.

in the PICA layer and can this data be used to estimate the depth of the char layer in the PICA, 3) what is the state of the bond-line between the aluminum honeycomb and the PICA layer, and 4) are there any features in this data that result from the scanning and processing techniques, themselves, and how could these techniques be improved upon for scanning another shield.

4. MEASUREMENT OF PICA THICKNESS

While there are many ways to measure the thickness of the PICA layer in the scanned volume, the methods developed here focus on “point-wise” techniques. That is, we sought to obtain measurements of the thickness of the PICA from points on the surface of the PICA. Unlike “shell-extraction” techniques, or “boundary-fitting” techniques, these methods do not fit to the elliptical shape, but rather attempt to measure boundaries as they are in the data, and calculate the difference between the boundaries. Our procedure starts with a “center vertical slice” and then rotates the volume to obtain measurements from “center vertical slices” at a large number of angles throughout the volume. In this way thickness measurements are obtained over the entire surface of the Stardust Shield.

The measurement procedure for a center vertical slice involves three steps; 1) measure the coordinates of the boundary of the outer PICA layer from the center vertical slice, 2) for the same vertical slice, measure the boundary of the inner PICA layer (the inner boundary is bounded by the aluminum honeycomb layer), and 3) measure the distance from outer to inner boundary on the line perpendicular to the surface of the outer boundary. Fig. 8 shows plots of the outer and inner boundary contours of the PICA layer from the scan of the Stardust shield obtained from “shrink-wrap” operations applied to the volume. Fig. 9 shows the PICA thickness measured from the boundaries in Fig. 8 compared with the “as-built” thickness. Fig. 10 shows the estimated material loss based on Figs. 8 and 9.

A few trends in the material loss in the PICA are apparent from the data. First the loss of material (compared to the assumed build with a constant thickness) is greater at the top of shield than towards the outer ends. The maximum loss is around 6.3 mm ($\frac{1}{4}$ inch) in thickness. But as can be seen from the outside of the shield there is substantial variation in the outer texture with “chunks” of the shield missing, possible due to the impact at landing. However, independent of the chunks missing from the shield, there appears to be a near-linear decrease in the loss of the PICA material proceeding from the top of the Shield to the outside edges.

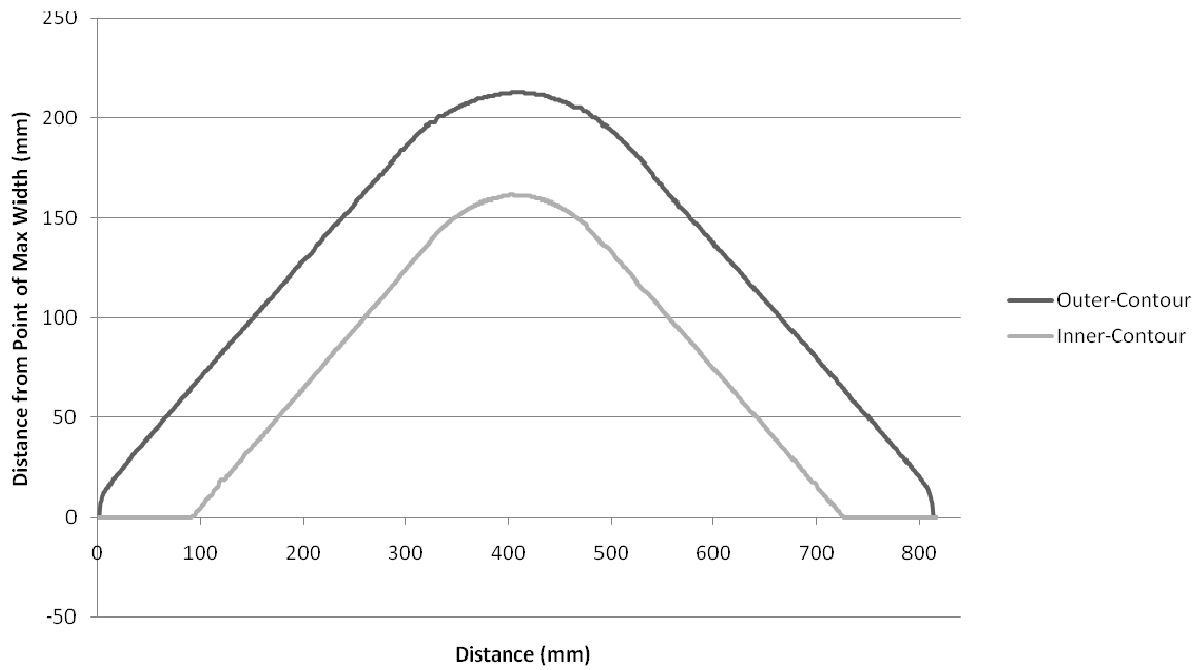


Fig. 8 – Plot of inner and outer boundaries of PICA.

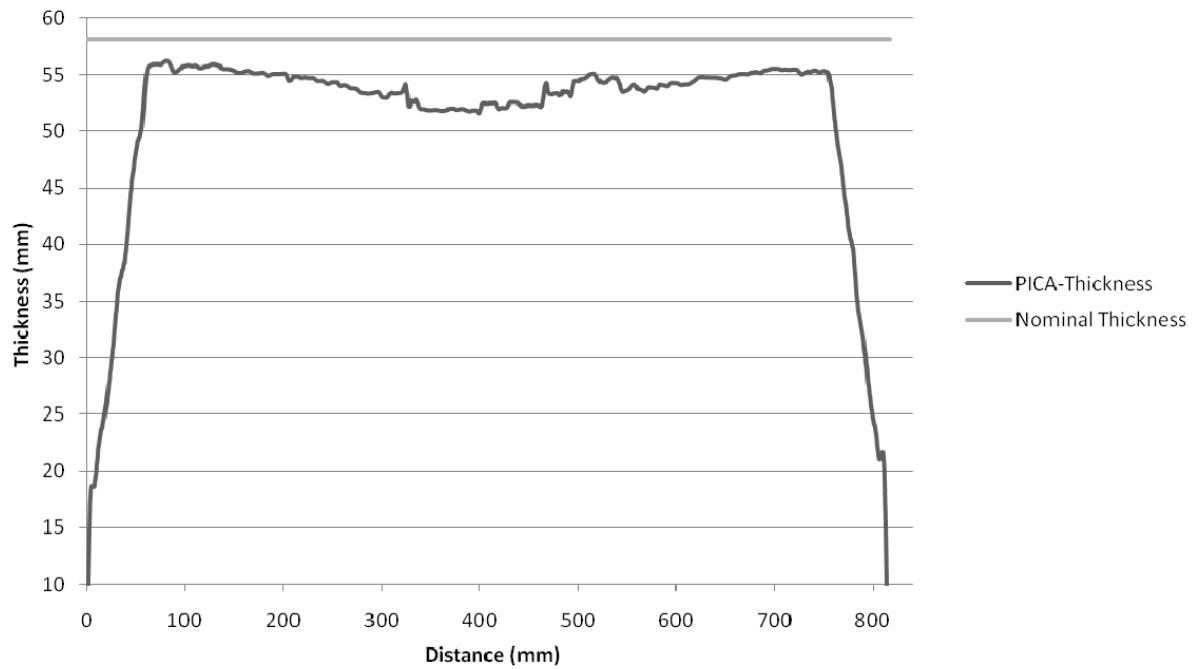


Fig. 9 – PICA thickness measurements.

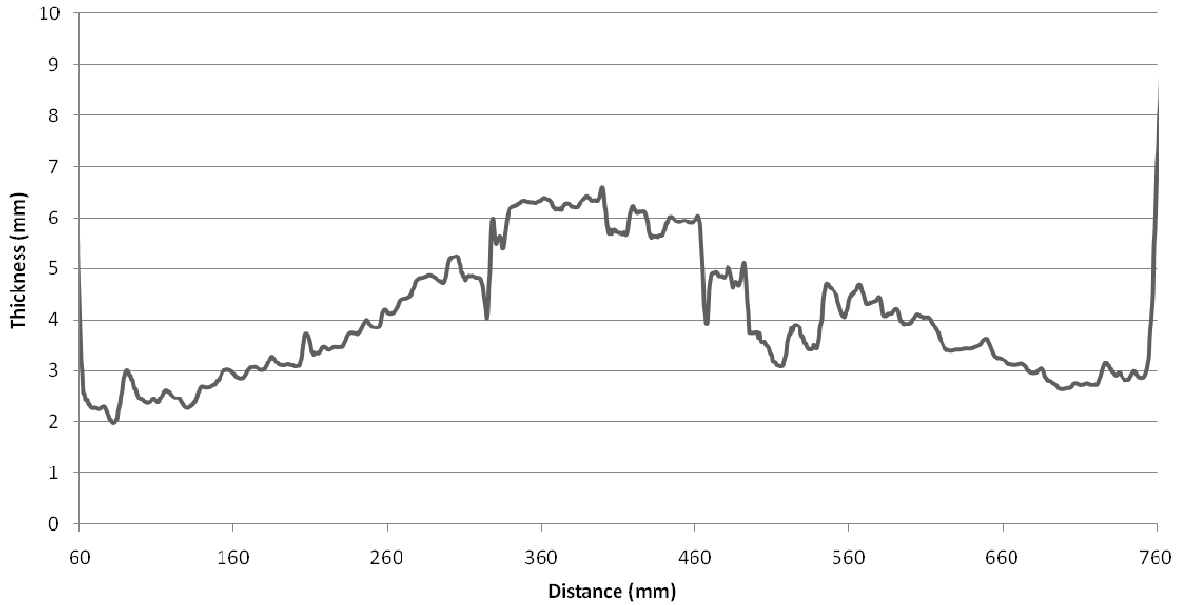


Fig. 10 - PICA thickness loss from nominal thickness of 58 mm.

Applying this technique to the entire volume involves rotating the scanned volume of the Stardust shield, and obtaining a sequence of center slices at different rotational angles. Independent of the debris sticking to the outside of the shield, and small variations in the surface of the shield, the trends in the thickness are reasonably consistent with the indications reported from a single slice. The center of the shield lost more material than the outer radii of the shield. These measurements show a material thickness loss of 6-6.5 mm in the top of the shield apex, and a low as 3 mm loss close to the outside radii of the shield surface. The variation in the material loss from top of the dome to the outer ends is only slightly non-linear, with the loss in material greatest at the dome, with a more rapid decrease from top of the dome to the ends, then less loss at the ends. It should be mentioned here that the drilled holes in the shield complicate these point-wise measurements from the CT data, where we are calculating “tangents” to contours and inverse slopes to the tangents, which in itself can be unstable (small values of the tangent results in large numbers in the inverse).

5. MEASUREMENTS OF THE CHAR LAYER

The “char” layer is a lower attenuating band of PICA material at the outer boundary of the shield. Fig. 11 includes an image extracted from the top of the dome, with the grey-level-window set to just span the attenuation of the PICA (the “dirt” on the outside layer are all at the maximum gray level). Notice the subtle differences in density characteristic of this layer. To

obtain a quantitative measure of the density differences in the charred PICA line-outs were acquired at different positions indicated on the image. Fig. 12 is a comparison of the relative attenuation along the line outs. Since the char layer occupies the region close to the outside boundary, we obtained “shell-extractions” from the reconstructed volume. This process involves finding the outer boundary, then shrinking the outer boundary to intersect a layer at a uniform distance from the edge, thereby generating an image of the internals of the Stardust shield in exclusively in the char layer. Fig. 13 is an image of the shell extraction of the entire char layer, Fig. 14 is a extract of the char layer shell, and Fig. 15 is an extract of a layer deeper into the PICA.

The variation in the attenuation values in the above images and displayed in the, images, line-outs, and histograms shows the difficulty in accurately dimensioning the char layer. First, there is variation in the fibers themselves that is close to the change in density in the char layer (0.000109 for a mean value of 0.00214 – approx 1 part in 20). Second, comparing average values from a shell extraction in the char layer and from a layer inside the char (the “no-char” region), the “char layer is lower in attenuation by about 12%. However, referring to Fig. 17, notice the substantial overlap between the histograms of voxels from the char and no-char layer. This can also be observed in the images; some of the fibers in the char layer retain their original density.

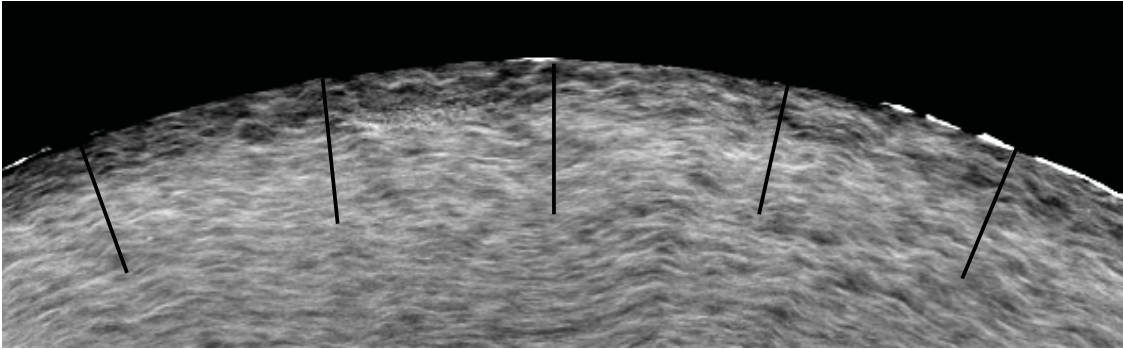


Fig. 11 - Extracted section of top dome showing approximate positions of line-outs.

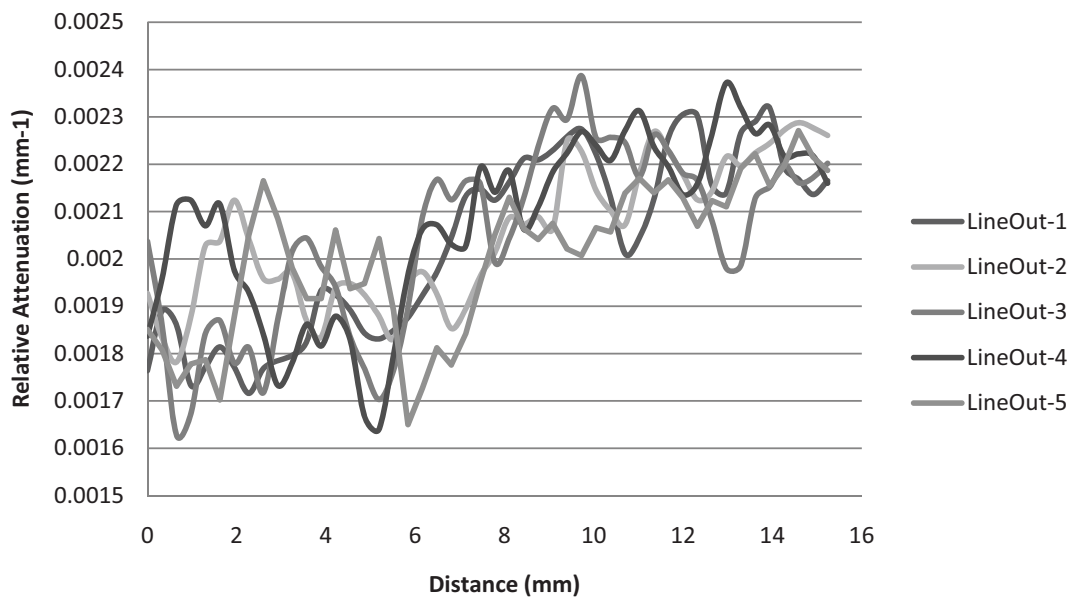


Fig. 12 - A comparison of the relative attenuation from the line-outs indicated in Fig. 11.

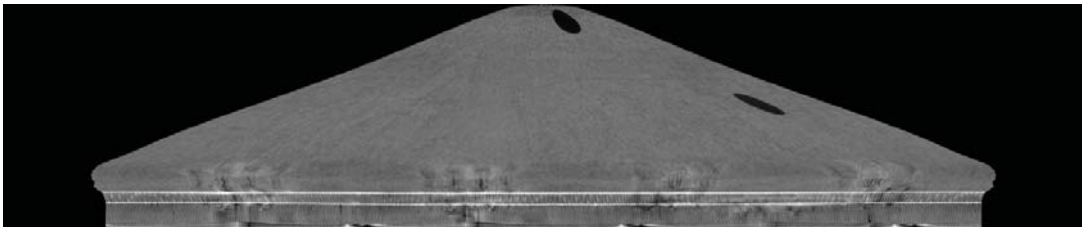


Fig. 13 - Shell extraction for the entire volume in the outer char layer.

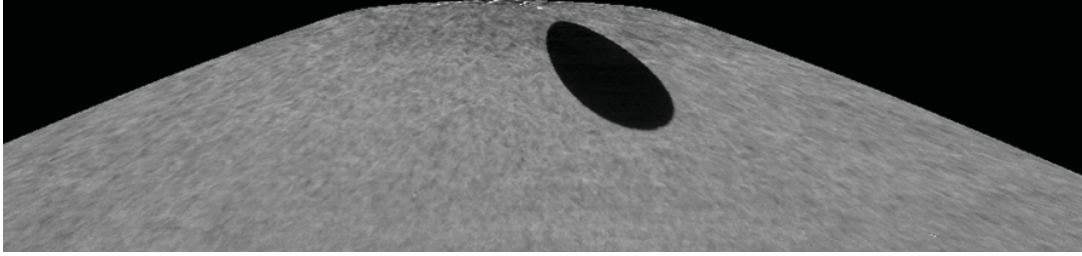


Fig. 14 – Extracted region from the shell of the outer char layer.

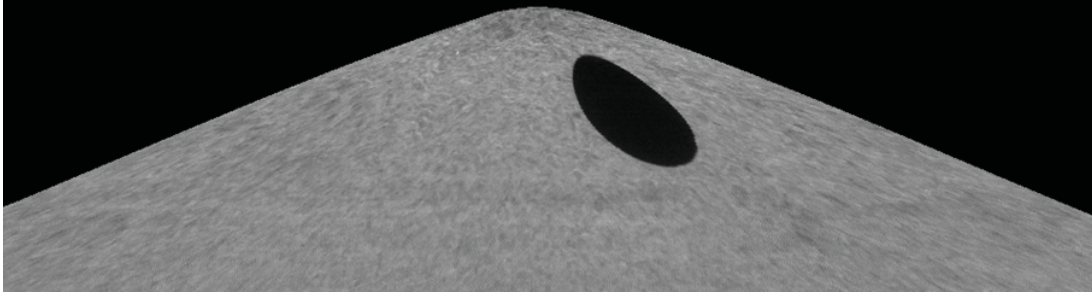


Fig. 15 - Extracted region from the shell of the inner layers of PICA well inside the char layer.

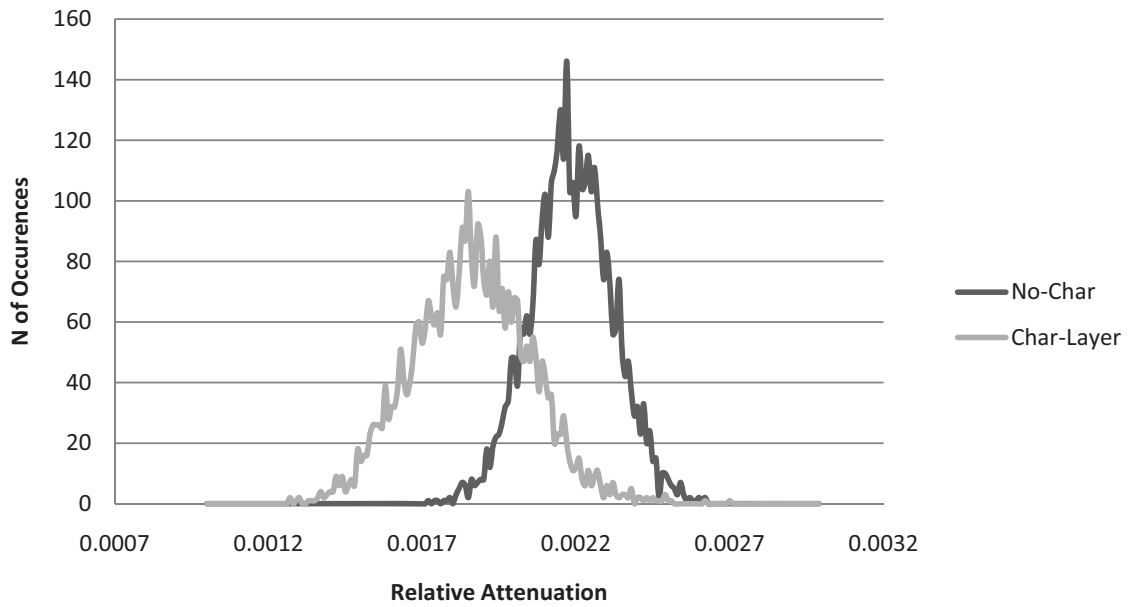


Fig. 16 - Histograms from extracted regions of the same size from the shell extraction data.

Third, and as expected, the loss in density in the char layer results in a material that is less uniform than the “no-char” region as shown in the width of the histogram for the “Char-Layer” voxels.

Using the shell extractions we can average along radial lines, effectively taking line-outs to obtain some measure of the depth of the char layer. Average depth of the char layer is 9.8 mm +/- 1mm. Also on average the char layer is greater at the positions of largest mass loss, that is, at the “dome” region of the Stardust Shield. Given all the difficulties mentioned above for distinguishing the char layer from the “no-char” layer, and the variation in the density of the PICA, this is admittedly a measurement with substantial local variation.

Comparisons of the above numbers with those from the cores taken from the heat shield are of interest. Reference [2] estimated the combined char layer and pyrolysis depth to be ~ 11 mm for the flank core and ~9 mm for the stagnation core, similar to the numbers above.

6. STRUCTURE AND ANOMALIES IN THE BOND LAYER

The “bond-layer” referred to here is the layer of material in-between the PICA and the Aluminum honeycomb. From the cross-sectional slices presented above and below the layer is higher in attenuation than the PICA, and is close in attenuation to the Aluminum. Figure Figs. 17 and 18 contain extracted regions from cross-sectional slices through the PICA, the section at the top of the honeycomb and containing the bond-layer. Notice the small porosity at about 4 o’clock in the bond-layer in Fig. 17. Also, notice the excess metal in the honeycomb.

The cross-sectional slice in Figure 18 shows a gap in the bond-layer at a radial position of 3 o’clock. This void-space in the “bond-layer” extends a length of approximately 20 mm at this particular position.

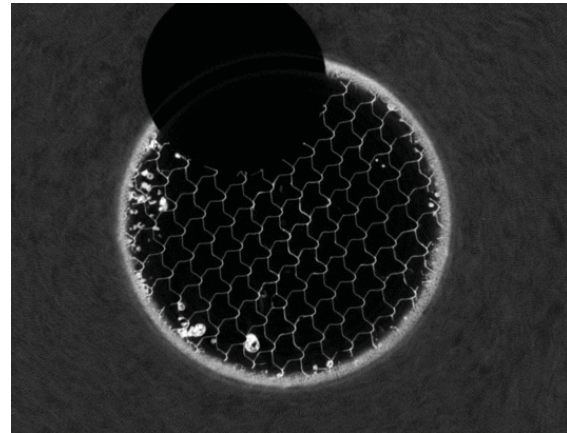


Fig. 17 - Cross-sectional slice showing PICA, bond-layer and Honeycomb.

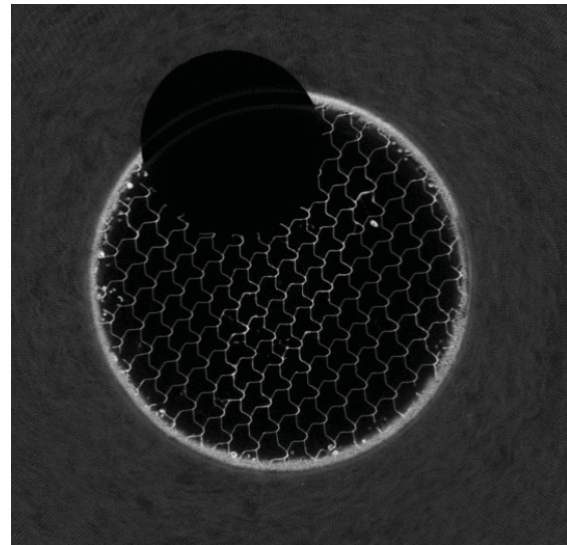


Fig. 18 - Cross-sectional slice showing a gap in the bond-layer.

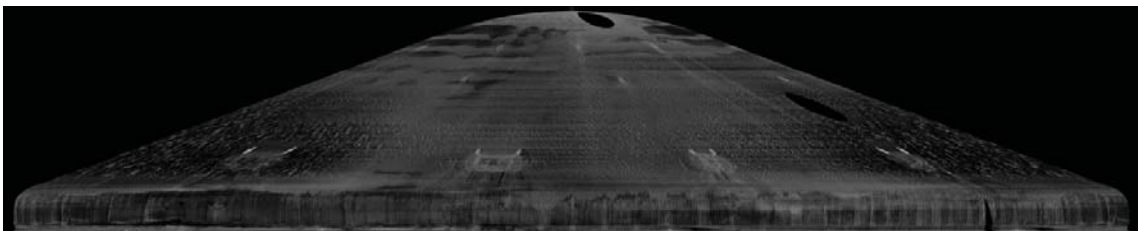


Fig. 19 - Shell extraction of the bond-layer.

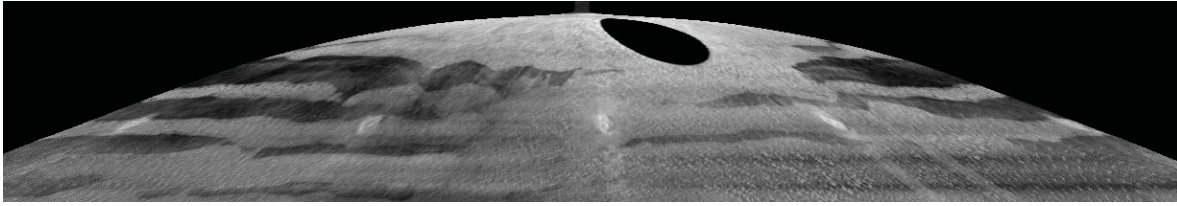


Fig. 20 - Close-up of the top of the image in Fig. 19.

“Shell extractions” utilized above to examine the char layer can be used to evaluate the bond-layer in the Stardust heat shield. Using the exterior of the aluminum honeycomb as a boundary we can position a shell with this contour in the geometric position of the “bond-layer”. Consequently, we obtain an image of the entire “bond-layer” in one image. Figs. 19 and 20 show this.

The “shell-extraction” images show a number of gaps in the “bond-layer” in the Stardust heat shield. In general the bond-line is better filled at the top of the shield than down the length towards the ends of the shield. In particular for the section at the top shown in Fig. 20 the bond-layer is only 62% filled, that is 38% of the space in the bond layer contains substantial voids. At this point in time these results have not been compared to the as-built data so it is not clear if the void-fraction developed over time in service, or the void-fraction is as-built

7. ARTIFACTS IN THE CT DATA AND LESSONS LEARNED

From the evaluation of the entire 3D CT volume two different types of artifacts can be identified which hamper the evaluation of certain features in the data. First, the sections of PICA and aluminum honeycomb in close proximity to the Aluminum support structure are inundated with troublesome “streak” artifacts. Fig. 21 contains a cross-sectional slice displaying these effects in the reconstructed volume. These artifacts are the result of a “lack of penetration” of the longer sections of Aluminum in the support structure combined with the proportion of “Background Scatter” [3] characteristic of this technique. In many cases these effects can be remediated by a thicker x-ray beam filter, thereby increasing the average energy used in the scanning. This should be considered in subsequent scanning.

Another type of artifact occurs in the sections of the Stardust Shield down from the top of dome and is due to the lack of views acquired. There is a relationship between the radius at which features appear and the angular increment used to obtain the number of views for the reconstruction [4]. In particular, the angular

increment must be comparable with the spatial resolution of the radiographic projection to get all the

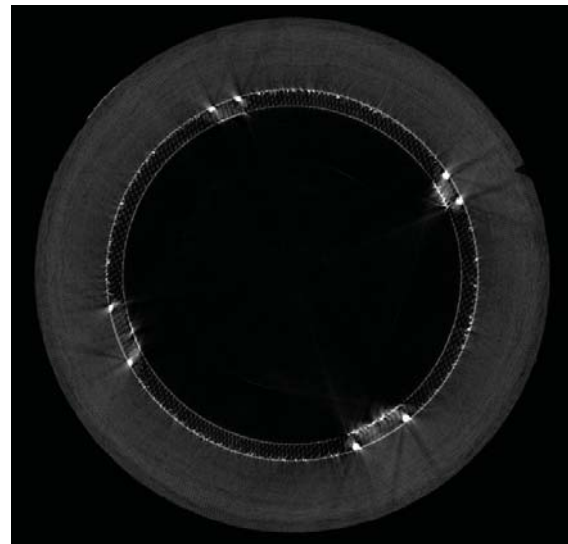


Fig. 21 - Cross-sectional slice showing streak artifacts.

resolution available in the radiograph into the 3D reconstruction. The mathematics result in the requirement that the number of rotational views be π or $\pi/2$ times the number of spatial resolution elements out to the radius of interest. Given that the PICA is at a radius of some 900 pixels, it is clear that 900 views are not adequate to avoid the periodic noise resulting from the lack of rotational views. The result is an additional source of noise that makes detailed examination of the PICA in the wider sections of the shield more difficult. In subsequent scans the number of views should be increased to 1200 or 1800 views over 360, provided part-availability and funding exist for this added scan time.

8. SUMMARY

To evaluate the structure of the Stardust Shield a tiled-CT scan was performed on the Stardust Shield in the newly fabricated 450 kVp x-ray room at JSC. The results are varied. First, the results show the loss in the shield thickness as compared to the as-built thickness to be 6-6.5 mm in the top of the shield apex, and a low as 3 mm loss close to the outside radii of the shield surface. The variation in the material loss from top of the dome to the outer ends is only slightly non-linear, with the loss in material greatest at the dome, with a more rapid decrease from top of the dome to the ends, then less loss at the ends. Second, CT data showed indications of a char layer in the PICA on the outside of the Stardust Shield. The density of the char layer is less than the unaffected PICA by 12%. Also, the thickness of the char layer is on average 9.8 mm +/- 1 mm. This measurement includes substantial local variations with some of the fibers in the char layer near the attenuation values of the unaffected PICA. The nature of this variation is difficult to establish without better data on the as-built material. Lastly, a few troublesome scan artifacts were identified as part of these scans. We recommend a thicker x-ray beam filter and the acquisition of more rotational views. For tiled-CT scanning increasing the number of rotational views increases the scan time by the number of tiles, and could result in substantial increased cost. However, if the interest of the scan is focused on the top of the dome where the angular increment and radius requirements are not as stringent, this scan strategy is adequate to support the variety of measurements presented here.

The final recommendation, for future probes requiring TPS (and returning to Earth), would be to perform a similar CT scan before launch in order to have "before" and "after" measurement for comparison. Some of the values reported in this paper have significant uncertainty due to lack of exact pre-flight configuration data. As-built information and construction drawings were consulted but the fine detail available from the tomography were absent resulting in less accuracy than desired.

9. REFERENCES

1. Empey D. M. and Schneberk, D. J., *Results from medium resolution and high resolutions scans of PICA*, Working Paper, 2007
2. Stackpoole M., Sepka S., Cozmata I., Kontinos D., *Post-Flight Evaluation of Stardust Sample Return Capsule Forebody Heatshield Material*, AIAA-2008-1202, 46th AIAA Aerospace Sciences Meeting and Exhibit, Reno, Nevada, 2008
3. Schneberk, D. J. and Martz, H., *Radiographic Testing*, ASNT Press, 2002
4. Kak A. C. and Slaney M., *Principals of Computerized Tomographic Imaging*, IEEE Press, New York, 1987